Chemical Research in Toxicology

Article

pubs.acs.org/crt

On the Reaction Mechanism of Tirapazamine Reduction Chemistry: Unimolecular N−OH Homolysis, Stepwise Dehydration, or Triazene Ring-Opening

Jian Yin,[†] Rainer Glaser,*[,†] and Kent S. Gates*[,†,‡]

Departments of [†]Chemistry and [‡]Biochemistry, University of Missouri, Columbia, Missouri 65211, United States

Supporting Information

ABSTRACT: The initial steps of the activation of tirapazamine (TPZ, **1**, 3-amino-1,2,4-benzotriazine 1,4-*N*,*N*-dioxide) under hypoxic conditions consist of the one-electron reduction of **1** to radical anion **2** and the protonation of **2** at O(N4) or O(N1) to form neutral radicals **3** and **4**, respectively. There are some questions, however, as to whether radicals **3** and/or **4** will then undergo N−OH homolyses **3** → **5** + ·OH and **4** → **6** + ·OH or, alternatively, whether **3** and/or **4** may react by dehydration and form aminyl radicals via **3** → **11** + H_2O and **4** → **12** + H_2O or phenyl radicals via **3** → **17** + H_2O. These outcomes might depend on the chemistry *after the homolysis* of **3** and/or **4**, that is, dehydration may be the result of a two-step sequence that involves N−OH homolysis and formation of ·OH aggregates of **5** and **6** followed by H-abstraction within the ·OH aggregates to form hydrates of aminyls **11** and **12** or of phenyl **17**. We studied these processes with configuration interaction theory, perturbation theory, and density functional theory. All stationary structures of OH aggregates of **5** and **6**, of H_2O aggregates of **11**, **12**, and **17**, and of the transition state structures for H-abstraction were located and characterized by vibrational analysis and with methods of electron and spin-density analysis. The doublet radical **17** is a normal spin-polarized radical, whereas the doublet radicals **11** and **12** feature quartet instabilities. The computed reaction energies and activation barriers allow for dehydration in principle, but the productivity of all of these channels should be low for kinetic and dynamic reasons. With a view to plausible scenarios for the generation of latent aryl radical species *without* dehydration, we scanned the potential energy surfaces of **2**−**4** as a function of the (O)N1−Y (Y = C5a, N2) and (O)N4−Z (Z = C4a, C3) bond lengths. The elongation of any one of these bonds by 0.5 Å requires less than 25 kcal/mol, and this finding strongly suggests the possibility of bimolecular reactions of the spin-trap molecules with **2**−**4** concomitant with triazene ring-opening.

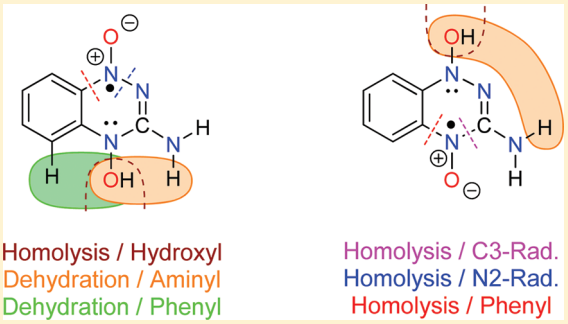

INTRODUCTION

Tirapazamine (TPZ, **1**, 3-amino-1,2,4-benzotriazine 1,4-*N*-dioxide) selectively damages the DNA of solid tumor cells under hypoxic conditions.[1] The mechanism of TPZ-mediated DNA strand cleavage has been studied extensively using experimental and theoretical approaches by the groups of Laderoute,[2−5] Lloyd,[6] Patterson,[7] Gates,[8−15] Anderson,[16−18] and Li,[19] and several mechanistic proposals have been advanced concerning the identities of the toxicologically active species and their formations. There exists general agreement that one-electron reduction of **1** gives **2** and that **2** may be protonated to **3** and/or **4**. Questions remain regarding the subsequent chemistry.

The first question concerns the nature of the reactive species generated from **3** and/or **4**. One option is homolysis leading to **5** and/or **6** and the formation of reactive OH radicals. The alternative is dehydration of **3** and/or **4** and the formation of reactive organic radicals of the types **11**, **12**, **17**, and **18**. In the latter case, the additional question arises as to whether the dehydration is a concerted or a stepwise process.

In normally oxygenated cells, the primary TPZ metabolite **2** (3-amino-1,2,4-benzotriazine 1,4-*N*-dioxide anion) is rapidly oxidized back to **1**. The radical anion **2** has been detected by EPR spectroscopy,[6,18] and all interpretations agree that the radical is mostly located in the (N1,O) region. In the hypoxic environment of solid tumors, the anion radical **2** has a longer lifetime and can be protonated to form the neutral isomeric radicals **3** and/or **4**, respectively.[2,4,5] Laderoute, Wardman, and Rauth considered the C3-centered radical to be most important (LWR radical) based on semiempirical computations,[2] whereas Lloyd et al. argued in support of the *N*-centered nitroxide radical (LDRMB radical),[6] and higher level electron and spin-density analysis provided strong evidence in support of the latter.[20]

It is one option for **3** and/or **4** to undergo N−OH bond homolysis, and the hydroxyl radical[8,13,14] is a well-known DNA damaging agent.[21] Patterson and Taiwo detected the hydroxyl adduct of the spin-trap DMPO (5,5-dimethyl-1-pyrroline *N*-

Received: December 14, 2011
Published: March 5, 2012

dx.doi.org/10.1021/tx200546u | *Chem. Res. Toxicol.* 2012, 25, 634−645

Scheme 1. Overview of Proposed Mechanisms for TPZ Activation

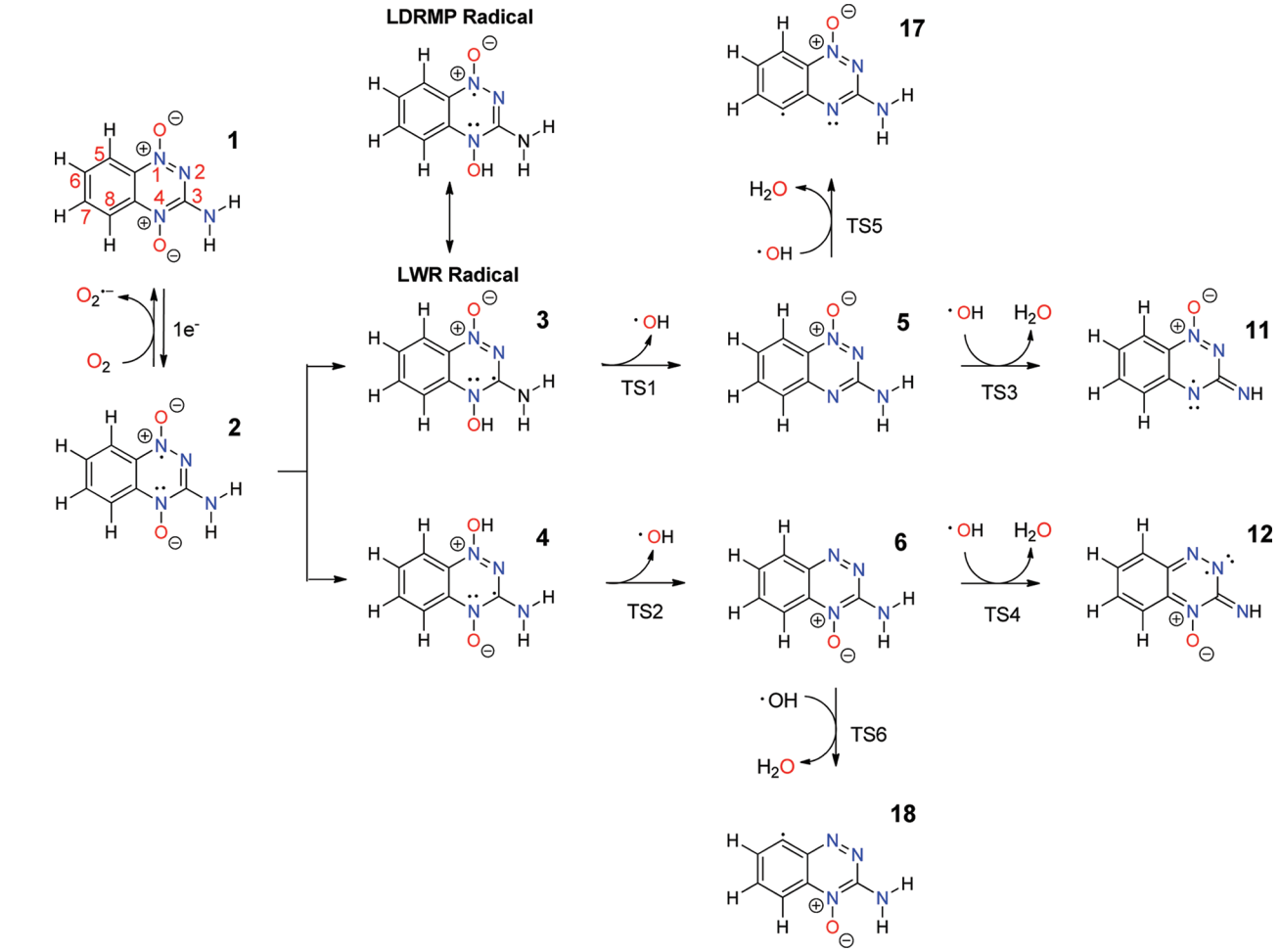

Scheme 2. Stepwise Dehydration of 3 May Involve N−OH Homolysis and Aggregate Formation between 5 and OH Followed by H-Abstraction and Formation of Hydrates 9 and/or 15

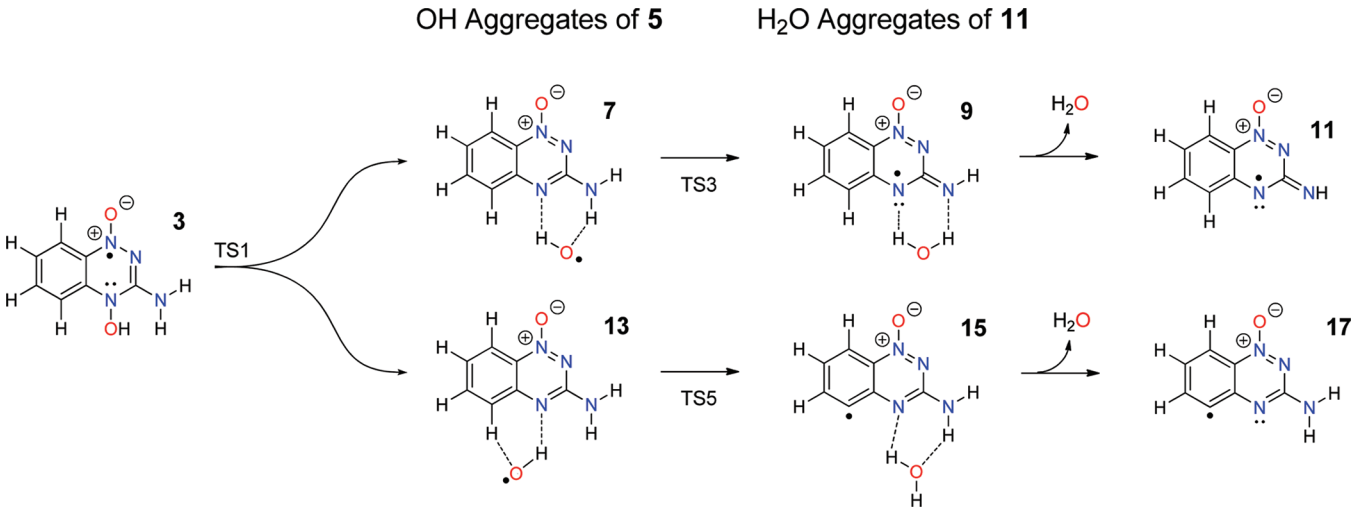

oxide) indicative of ·OH formation under these conditions.[7] A carbon-centered radical DMPO-R also was detected, but it was unclear whether this radical was formed by the addition of DMPO to **3**, **4**, or other species (i.e., DMSO).[7] The ·OH loss from **3** and/or **4**, respectively, leads to the formation of isomers **5** and/or **6** of neutral, closed-shell 3-amino-1,2,4-benzotriazine monoxide, and isomers **5** and **6** have been identified in previous studies.[10,22]

As an alternative to simple N−OH homolysis, Anderson and co-workers recently discussed the concerted dehydration of **3** which may lead to the benzotriazinyl radical **11** (BTZ)[17] and/or the aryl radical **17**.[17,18] The analogous dehydration of isomer

dx.doi.org/10.1021/tx200546u | *Chem. Res. Toxicol.* 2012, 25, 634−645

Table 1. Relative Isomer Stabilities and Activation Energies Computed at the B3LYP/6-31G* and QCI/6-31G*//B3LYP/6-31G* Levels

	DFT				QCI//DFT	
parameter	ΔE	ΔH_0	ΔH_{298}	ΔG_{298}	$\Delta E'$	$\Delta G'$
			OH Loss			
E_{rel}, **6** vs **5**	13.07	12.58	12.58	12.68	12.42	12.03
E_{rxn}, **3a** → **5** + **OH**	5.53	1.87	2.30	−7.74	0.52	−12.75
E_{rxn}, **4b** → **6** + **OH**	19.86	16.08	16.40	6.58	11.54	−1.74
E_{act}, **TS1** vs **3a**	6.45	4.99	4.86	5.01	13.05	11.61
E_{act}, **TS2** vs **4b**	14.88	12.88	12.96	12.63	20.75	18.50
			Water Loss, I			
E_{rel}, **11b** vs **11a**	0.53	0.50	0.52	0.47	0.35	0.29
E_{rel}, **12b** vs **12a**	0.90	0.94	0.97	0.82	1.32	1.24
E_{rel}, **12a** vs **11a**	0.40	0.47	0.54	0.38	−2.24	−2.26
E_{rxn}, **3a** → **11a** + H_2O	−5.13	−9.46	−9.00	−19.86	−5.61	−20.34
E_{rxn}, **4b** → **12a** + H_2O	−3.47	−7.37	−6.93	−17.84	−9.25	−23.62
E_{Agg}, **5** + **OH** → **7**	−12.69	−10.64	−10.60	−2.44	−6.41	3.84
E_{Agg}, **11** + H_2O → **9**	−7.46	−5.75	−5.22	2.29	−7.72	2.03
E_{Agg}, **6** + **OH** → **8**	−12.45	−10.47	−10.39	−2.33	−10.63	−0.51
E_{Agg}, **12a** + H_2O → **10**	−7.39	−5.64	−5.14	2.38	−5.76	4.01
E_{act}, **7** → **TS3**	9.65	6.52	6.19	7.00	24.18	21.53
E_{rxn}, **7** → **9**	−5.43	−6.45	−5.92	−7.39	−7.43	−9.39
E_{act}, **8** → **TS4**	5.66	2.85	2.60	3.13	24.95	22.42
E_{rxn}, **8** → **10**	−18.27	−18.62	−18.08	−19.71	−15.91	−17.35
			Water Loss, II			
E_{rxn}, **3a** → **17** + H_2O	9.52	5.70	6.44	−4.79	9.39	−4.92
E_{Agg}, **5** + **OH** → **13**	−10.01	−8.12	−7.92	0.01	−9.17	0.85
E_{Agg}, **17** + H_2O → **15**	−13.06	−10.44	−10.50	−1.13	−13.11	−1.18
E_{act}, **13** → **TS5**	13.97	9.64	9.62	10.14	25.22	21.39
E_{rxn}, **13** → **17** + H_2O	14.00	11.95	12.06	2.93	18.04	6.97

4 would lead to radicals **12** and **18**. Anderson argued that the presumed DMPO−OH spin-trap adduct was not formed by OH addition to DMPO but instead is the result of oxidation of DMPO to $DMPO^{\bullet+}$ and subsequent hydration and deprotonation[23] and showed that no OH adduct is formed with the spin-trap DEPMPO (5-(diethoxyphosphoryl)-5-methyl-1-pyrroline *N*-oxide).[17] More recently, Anderson and co-workers studied the reactions of the putative intermediate **3** with the spin-trap PBN (*α*-phenyl *N*-tertiary-butyl nitrone), and the EPR spectra were assigned to radicals formed by addition of PBN to C3 of **3** and to C8 of the aryl radical **17**.[17,18] Anderson's group explored the B3LYP/6-311+G(d,p) potential energy surface with focus on isomer **3** and reported reaction enthalpies ΔH_0 of the homolysis reaction **3** → **5** + ·OH and of the two dehydration reactions leading to radicals **11a** (**11a** = (*Z*)-**11**) or **17**. The reaction **3** → **5** + ·OH was predicted to be endothermic by ΔH_0 = 2.2 kcal/mol, the formations of BTZ radical **11a** to be exothermic by 10.9 kcal/mol, and the dehydration of **3** to phenyl radical **17** to be slightly endothermic by 0.5 kcal/mol, respectively.[18] The same reaction channels also were explored for four TPZ analogues **3-X** in which the amino group at C3 was replaced (X = H, CH_3, Ph, and OMe), and very similar scenarios were found: the N−OH homolyses of **3-X** are endothermic by 1.6 ÷ 5.9 kcal/mol, the formations of the BTZ-X analogues all are exothermic (ΔH_0 = −1.7 ÷ −19.4 kcal/mol), and the formations of the analogous phenyl radicals are slightly endothermic (0.0 ÷ 4.6 kcal/mol).

It is our premise that there may not be a fundamental difference between the mechanistic proposals of N−OH homolysis and dehydration and, instead, that the outcomes might depend on the chemistry after homolysis of **3** and/or **4**. Dehydration may be the result of a two-step reaction sequence that involves unimolecular N−OH homolysis and subsequent H-abstraction by ·OH (Scheme 1), and this is illustrated in more detail for the dehydration reactions of **3** in Scheme 2.[24] The homolysis of **3** (or **4**) would form aggregate **7** (or **8**) between the OH radical and **5** (or **6**) and subsequent H-abstraction would lead to aggregate **9** (or **10**) between water and **11** (or **12**). In analogy, the homolysis of **3** (or **4**) might form aggregate **13** (or **14**) between the OH radical and **5** (or **6**), and subsequent H-abstraction from the arene could then lead to aggregate **15** (or **16**) between water and **17** (or **18**). To test this premise, we have explored the stepwise paths for the dehydrations **3** → **11** + H_2O and **4** → **12** + H_2O as well as the dehydration **3** → **17** + H_2O. In light of the results obtained for the two dehydration modes of **3**, the dehydration of **4** → **18** + H_2O was not studied. The dehydration reactions were studied with the same theoretical methods which were employed in the study of **1**−**6** in the preceding article[20] (density functional theory, perturbation theory, and configuration interaction theory). While the computed reactions energies and the activation barriers (rate constants) allow for the dehydration reactions in principle, we will discuss kinetic and dynamic reasons that diminish the productivity for the dehydration paths and especially for the path to aryl formation. Scans of the potential energy surfaces of **2**−**4** as a function of the (O)N1−Y (Y = C5a, N2) and (O)N4−Z (Z = C4a, C3) bond lengths are discussed, and their analysis points to the possibility of bimolecular reactions of the spin-trap molecules with **2**−**4** concomitant with triazene ring-opening.

dx.doi.org/10.1021/tx200546u | *Chem. Res. Toxicol.* 2012, 25, 634−645

Table 2. Relative Isomer Stabilities and Activation Energies Computed at the MP2(full)/6-31G* and QCI/6-31G*//MP2(full)/6-31G* Levels

	MP2				QCI//MP2	
parameter	ΔE	ΔH_0	ΔH_{298}	ΔG_{298}	$\Delta E'$	$\Delta G'$
			OH Loss			
E_{rel}, **6** vs **5**	13.64	13.05	13.05	13.12	14.05	13.53
E_{rxn}, **3a** → **5** + **OH**	−22.70	−29.95	−28.99	−40.06	−1.72	−19.08
E_{rxn}, **4b** → **6** + **OH**	−12.37	−20.11	−19.29	−29.98	11.54	−6.07
E_{act}, **TS1** vs **3a**	36.08	33.75	33.77	33.59	14.16	11.67
E_{act}, **TS2** vs **4b**	39.94	36.09	36.54	35.24	20.15	15.45
			Water Loss, I			
E_{rel}, **11b** vs **11a**	0.36	0.37	0.37	0.36	0.35	0.35
E_{rel}, **12b** vs **12a**	1.42	1.87	1.90	1.54	2.22	2.34
E_{rel}, **12a** vs **11a**	−3.38	−2.13	−2.02	−2.48	3.16	4.06
E_{rxn}, **3a** → **11a** + H_2O	21.52	15.54	16.19	5.02	−5.94	−22.44
E_{rxn}, **4b** → **12a** + H_2O	14.83	10.2	10.82	−0.51	−3.56	−18.90
E_{Agg}, **5** + **OH** → **7**	−11.71	−9.60	−9.55	−1.07	−11.17	−0.53
E_{Agg}, **11** + H_2O → **9**	−8.13	−6.39	−5.86	1.55	−7.71	1.97
E_{Agg}, **6** + **OH** → **8**	−11.81	−9.60	−9.61	−0.97	−10.59	0.25
E_{Agg}, **12** + H_2O → **10**	−8.25	−6.24	−5.78	1.91	−7.15	3.01
E_{act}, **7** → **TS3**	74.19	73.65	72.86	74.28	25.42	25.51
E_{rxn}, **7** → **9**	47.79	48.70	48.87	47.69	−0.76	−0.86
E_{act}, **8** → **TS4a**	72.83	72.36	71.58	73.15	27.00	27.32
E_{rxn}, **8** → **10**	30.75	33.68	33.93	32.36	−11.67	−10.06
			Water Loss, II			
E_{rxn}, **3a** → **17** + H_2O	−5.20	−8.99	−8.06	−19.70	9.40	−5.10
E_{Agg}, **5** + **OH** → **13**	−9.94	−7.93	−7.77	0.24	−9.30	0.88
E_{Agg}, **17** + H_2O → **15**	−12.26	−9.93	−9.89	−0.75	−12.54	−1.03
E_{act}, **13** → **TS5**	33.12	33.36	32.89	34.25	29.16	30.29
E_{rxn}, **13** → **17** + H_2O	27.44	28.89	28.70	20.12	20.42	13.10

COMPUTATIONAL METHODS

Calculations were carried out using the Gaussian 09 program[25] on a 64-processer SGI Altix system and a multivendor compute cluster with 170 compute nodes (Dell, IBM, ACT) and over 1000 Intel 64 Xeon processor cores.

Potential Energy Surface Analysis. All structures were optimized with the hybrid density functional method B3LYP[26] and with second-order Møller−Plesset perturbation theory (MP2),[27] and in conjunction with the 6-31G* basis set. Harmonic vibrational analyses were performed for all stationary structures at both levels and employed to compute vibrational zero-point energies (VZPE), thermal energies (TE), and molecular entropies (S). In the potential energy surface analyses, restricted wave functions were employed for closed shell systems (RB3LYP, RMP2) and unrestricted theory was employed (UB3LYP, UMP2) for open-shell systems. The results obtained at the B3LYP/6-31G* and MP2(full)/6-31G* levels are listed in Tables S1 and S2, respectively, as Supporting Information. The relative and activation energies computed at the B3LYP/6-31G* and MP2(full)/6-31G* levels, respectively, are reported in Tables 1 and 2, respectively. The reported data include energies ΔE, enthalpies at 0 K ($\Delta H = \Delta E + \Delta VZPE$) and 298 K ($\Delta H_{298} = \Delta E + \Delta TE$), and free enthalpies ($\Delta G_{298} = \Delta H_{298} - T{\cdot}\Delta S$).

We also performed single-point energy calculations with the configuration interaction method QCISD[28] using the same basis set and the B3LYP and MP2 optimized geometries, respectively. The QCI total energies are included in Tables S1 and S2 (Supporting Information), and Tables 1 and 2 contain $\Delta E'$ and $\Delta G'$ values computed with the QCISD energies. The $\Delta G'$ values include the thermochemical corrections computed at the level of optimization, that is, $\Delta G' = \Delta E' + (\Delta G - \Delta E)$.

Electron and Spin-Density Analysis. We discussed the concepts of electron and spin-density distributions in some detail in the preceding article,[20] and the ideas about spin-delocalization and spin-polarization[29−31] are relevant to the present study as well. Spin polarization intrinsically is an electron correlation effect, and the quality and reliability of spin-density distributions increases with the quality of the correlation treatment. To ensure that the spin densities are reliable requires the computation of highly correlated wave functions with variational correlation methods, and we employ the QCISD level as our standard.

We previously discussed spin-free singlet ground states of **1**, **5**, and **6** and the low-lying spin-polarized excited states **SP-1**, **SP-5**, and **SP-6**. One speaks of a "triplet instability" in cases of singlet states in which the biradical wave function is preferred over the closed-shell wave function and important examples include ozone, O_3,[32,33] some conjugated macrocycles,[34] fullerenes and nanotubes,[35] and nitro compounds and related species.[36] The term "triplet instability" is used to denote the number of unpaired electrons (biradical) and not necessarily the net spin (singlet or triplet). Here, we will encounter doublet radicals which exhibit a so-called "quartet instability." As with the use of the term "triplet instability," the term "quartet instability" denotes the number of unpaired electrons (triradical rather than a monoradical) and not the net spin (doublet or quartet).

In Tables 4 and 5 are listed the Mulliken spin populations and the Mulliken populations, respectively. In both tables, we report the results obtained at the QCI//DFT and QCI//MP2 levels. Spin populations for hydrogen atoms are included with the spin population of the atom to which the H atoms are attached. The values Σ_1 and Σ_2 provide the overall spin populations of the heterocyclic arc (N1−N2−C3−N4 with exocyclic attachments) and of the benzene ring (C4a−C5a−C5−C6−C7−C8 with attached H-atoms), respectively. To assess the overall extent of spin polarization, we define and report the parameters Σ_α and Σ_β, that is, the sums of the spin populations of all fragments with net α- or β-spin populations, respectively. Similarly, to assess the extent of charge distribution within the two ring systems, we define the parameters Θ_1 and Θ_2, respectively, in analogy to Σ_1 and Σ_2, respectively. To quantify the notion of "internal polarization," we define and the parameter Θ_+ as the sums the charges of all fragments

dx.doi.org/10.1021/tx200546u | Chem. Res. Toxicol. 2012, 25, 634−645

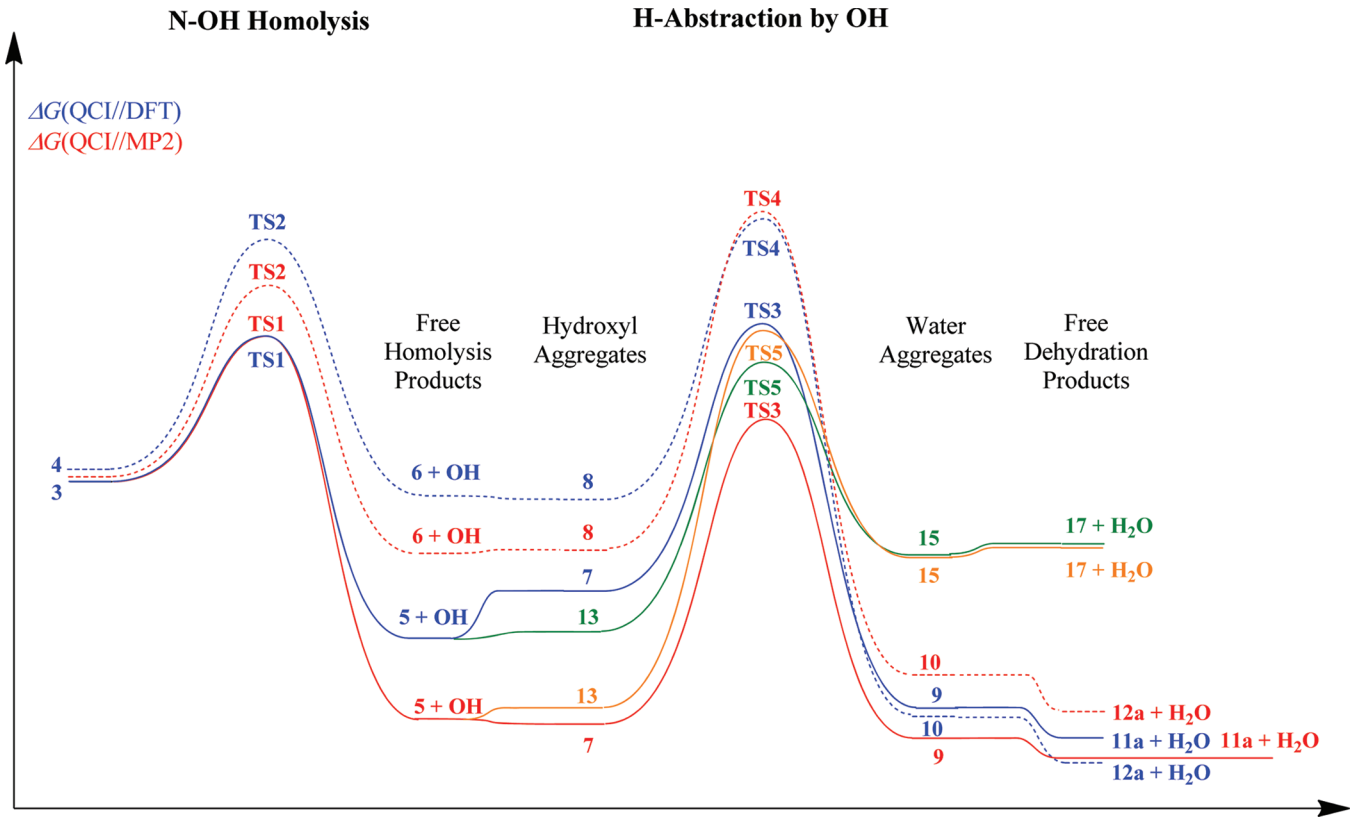

Figure 1. Free enthalpy surfaces for reactions of isomers **3** (solid) and **4** (dashed) as computed at the QCI//DFT (blue) and QCI//MP2 (red) levels. N−OH homolyses may lead to dehydration products if hydroxyl engages in hydrogen abstraction. In addition to the paths for the formation of aminyl radicals (blue, red), the paths for H-abstraction at C8 and formation of phenyl radicals are shown (green and orange). See text for details.

with net (+)-charge. In analogy, the parameter Θ_- equals the sums the charges of all fragments with net (−)-charge and $\Theta_- = -\Theta_+ - n$, where n is the overall charge of the system.

The analysis of spin-density distributions informs us about the relative importance of the various resonance forms, and QCI spin-density distributions are shown in Figure 3 for two values of ρ^S based on the MP2 and DFT structures. The surface plot computed with the higher setting of $\rho^S = 0.002$ e au^{-3} allows for the identification of the major radical sides and of the major mechanism of spin delocalization, while the lower setting of $\rho^S = 0.0004$ e au^{-3} reveals details of spin polarization. We discuss only QCI spin densities throughout this article and the spin-density distributions computed at the DFT and MP2 levels are provided in Supporting Information.

RESULTS AND DISCUSSION

N−OH Homolysis and Product Aggregation. We have previously discussed the free enthalpy surfaces of the N−OH homolysis reactions of isomers **3** (solid) and **4** (dashed), and the results obtained at the QCI//DFT (blue) and QCI//MP2 (red) levels are illustrated in the left part of Figure 1 based on the ΔG′ data. The QCI//DFT and QCI//MP2 activation barriers ΔG' for hydroxyl loss from **3** are 11.6 and 11.7 kcal/mol, respectively. By contrast, the activation barriers ΔG' for hydroxyl radical loss from **4** are 18.5 and 15.5 kcal/mol, respectively. The activation barriers computed at the QCI-level for the reaction via **TS1** are consistent with the experimental dissociation energy of ΔG_{exp} = 14 kcal/mol estimated in neutralization−reionization mass spectrometry experiments.[13]

The hydrogen abstraction by the HO radical, the second step of the stepwise dehydration of isomers **3** and **4**, respectively, begins with the hydroxyl-molecule aggregates **7** and **8** as substrates, proceeds via the hydrogen transfer transition state structures **TS3** and **TS4**, and leads to the hydrates **9** and **10** of the dehydration products **11** and **12**, respectively. In Figure 1, we show the energy levels of the hydroxyl aggregates to the right of the energy levels of the free homolysis products, and the respective levels are connected to guide the eye. Of course, the intrinsic reaction path for the dehydration of **3** (or **4**) would connect **TS1** (or **TS2**) directly to **7** (or **8**) and then on to **TS3** (or **TS4**).

It might seem odd that several aggregates are placed above the levels of the free constituents in Figure 1. The reaction *energies* ΔE and ΔE' for the aggregations **5** + OH → **7**and **6** + OH → **8** and the hydrate formations **11** + H_2O → **9** and **12** + H_2O → **10** all are negative (Tables 1 and 2). However, the aggregation *free enthalpies* ΔG and ΔG' are much less exothermic or even slightly endothermic because of the entropy loss upon association.

The products of N−OH homolysis may quickly separate after the transition state structure **TS1** has been traversed, and this outcome is most likely in gas phase. In solution, however, it is plausible that the separation of **5** and OH is slowed, that OH remains in the proximity of **5**, and that radical−molecule aggregate **7** is formed. Similarly, the homolysis reaction of **4** may lead to aggregate **8** after **TS2** is traversed. Molecular models of the B3LYP/6-31G* optimized structures of aggregates **7** and **8** are shown in Figure 2. The MP2/6-31G* structures look the same to the eye, and noticeable differences will be discussed.

The hydroxyl in **7** is well positioned for H-abstraction from the amino group of **5** and hydrate **9** can be formed via transition state structure **TS3**. The overall outcome of this sequence is the dehydration of **3a** to **11**; **3a** −(**TS1**) → **7**

dx.doi.org/10.1021/tx200546u | *Chem. Res. Toxicol.* 2012, 25, 634−645

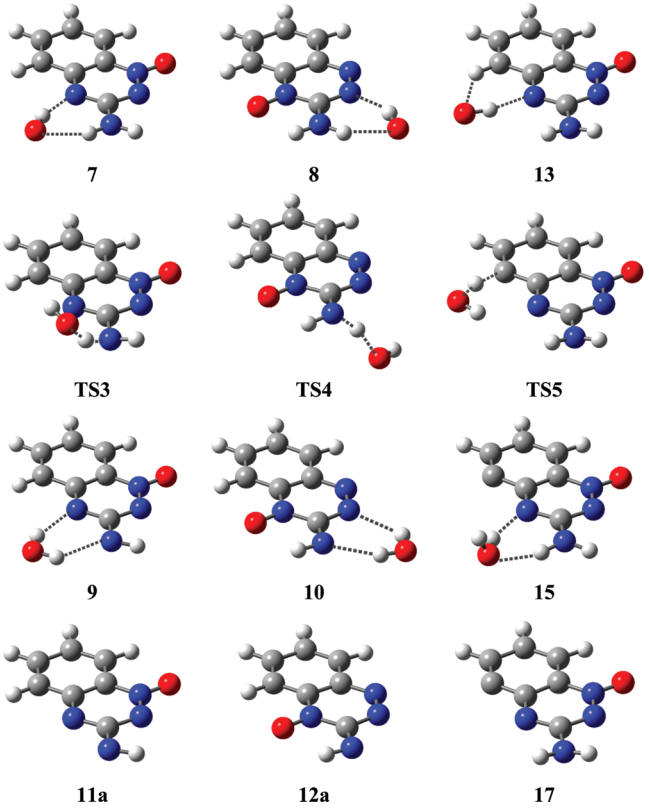

Figure 2. Stationary structures along the paths for dehydration of isomers **3** and **4** via stepwise, radical elimination mechanisms to products **11a**, **12a**, and **17**. The hydroxyl aggregates **7**, **8**, and **13** are the substrates for H-abstraction and lead to the product hydrates **9**, **10**, and **15**.

−(**TS3**) → **9** → **11a** + H_2O (Scheme 2). The analogous sequence of events for isomer **4** involves the path **4b** −(**TS2**) → **8** −(**TS4**) → **10** → **12a** + H_2O, where **8** is the aggregate **6**·(·OH), and **10** is the hydrate **12**·(H_2O). The respective stationary structures are shown on the left and center columns of Figure 2. The DFT-structure **TS4** shown in Figure 2 has its equivalent in structure **TS4a** on the MP2 level. On the MP2 potential energy surface, we also located a structure **TS4b** in which the hydroxyl-O is located more closely to N2 (Table 3). Paths exist from **4** to **10** that go through aggregates with short contacts between N2 and the hydroxyl-O, but these paths offer no energetic advantage.

An alternative to H-abstraction from the amino group in the hydroxyl-molecule aggregates **7** or **8** might involve the abstraction of a benzene-H and especially of the benzene-H which is closest to the N−OH bond that undergoes homolysis. The overall outcomes of these sequence are the dehydration of **3a** to **17** via the path **3a** −(**TS1**) → **13** −(**TS5**) → **15** → **17** + H_2O (Scheme 2) and the dehydration of **4b** to **18** via the path **4b** −(**TS2**) → **14** −(**TS6**) → **16** → **18** + H_2O. We studied this option for isomer **3**, and the respective structures are shown in the right columns of Figure 2.

Products of Dehydration: Aminyl-1,2,4-Benzotriazene Monoxides versus the Phenyl Radical. Phenyl radical **17** is a mostly localized σ-radical with only modest spin delocalization and/or spin polarization and no options for isomers. The aminyl systems are capable of forming geometrical isomers, and we studied the isomers **11a** and **12a** which result by abstraction of the amino-H that is close to the hydroxyl in aggregates **7** and **8**, respectively. Isomers **11a** and **12a** both are (*Z*)-configured, and they are slightly preferred over the respective (*E*)-isomers **11b** and **12b**, respectively, at all levels (Tables 1 and 2). The difference in the stabilities of isomers **11a** and **12a** is much less clear. The values computed at the levels of optimization have the opposite sign, and curiously, the QCI//DFT and QCI//MP2 data still have opposite signs, but the signs are reversed compared to the level of optimization. This pronounced theoretical level dependency indicates that the electronic structures of **11** and **12** must be very different.

Table 3. Selected Geometry Parameters Computed at DFT and MP2 Levels

molecule	distance	value	distance	value	distance	value
			DFT			
7	(O)H to N4	1.889	(H)O to $H(NH_2)$	2.069	N−H	1.017
8	(O)H to N2	1.944	(H)O to $H(NH_2)$	2.057	N−H	1.017
13	(O)H to N4	1.885	(H)O to H(C8)	2.598	C8−H	1.086
TS3	(O)H to N4	2.721	(H)O to $H(NH_2)$	1.254	N···H	1.177
TS4	(O)H to N2	2.947	(H)O to $H(NH_2)$	1.375	N···H	1.116
TS5	(O)H to N4	2.265	(H)O to H(C8)	1.156	C8−H	1.333
9	(O)H to N4	2.254	O−H	0.971	N···H	2.361
10	(O)H to N2	2.451	O−H	0.972	N···H	2.221
15	(O)H to N4	1.984	(H_2)O to $H(NH_2)$	1.940		
			MP2			
7	(O)H to N4	1.941	(H)O to $H(NH_2)$	2.166	N−H	1.015
8	(O)H to N2	1.996	(H)O to $H(NH_2)$	2.149	N−H	1.017
13	(O)H to N4	1.936	(H)O to H(C8)	2.614	C8−H	1.086
TS3	(O)H to N4	2.548	(H)O to $H(NH_2)$	1.172	N···H	1.227
TS4a	(O)H to N2	2.350	(H)O to $H(NH_2)$	1.245	N···H	1.158
TS4b	(O)H to N2	2.236	(H)O to $H(NH_2)$	1.169	N···H	1.341
TS5	(O)H to N4	2.401	(H)O to H(C8)	1.130	C8−H	1.330
9	(O)H to N4	2.135	O−H	0.969	N···H	2.682
10	(O)H to N2	2.495	O−H	0.972	N···H	2.206
15	(O)H to N4	2.050	(H_2)O to $H(NH_2)$	1.968		

The dehydration products **11a** and **12a** formally are aminyl radicals (**11A** and **12A** in Scheme 3), and delocalization of the unpaired electron gives rise to resonance forms with an exocyclic imine group. Allyl delocalization over the 1,3-diazaallyl system (blue shading) would place spin density on N4 in **11B** and **12B**. The **B** forms are aza-analogues of the benzyl radical (gray shading), and we show **11C** and **12C** to collectively refer to resonance forms that describe spin delocalization into the benzene ring. One major difference between the electronic structures of **11** and **12** concerns the possibility of delocalizing spin onto oxygen. Spin delocalization from N to O is easily possible in **12** (i.e., **12B** ↔ **12D**). However, spin delocalization onto O and/or N2 would require

dx.doi.org/10.1021/tx200546u | *Chem. Res. Toxicol.* 2012, 25, 634−645

Scheme 3. Electronic Structure of Radicals 11a and 12a

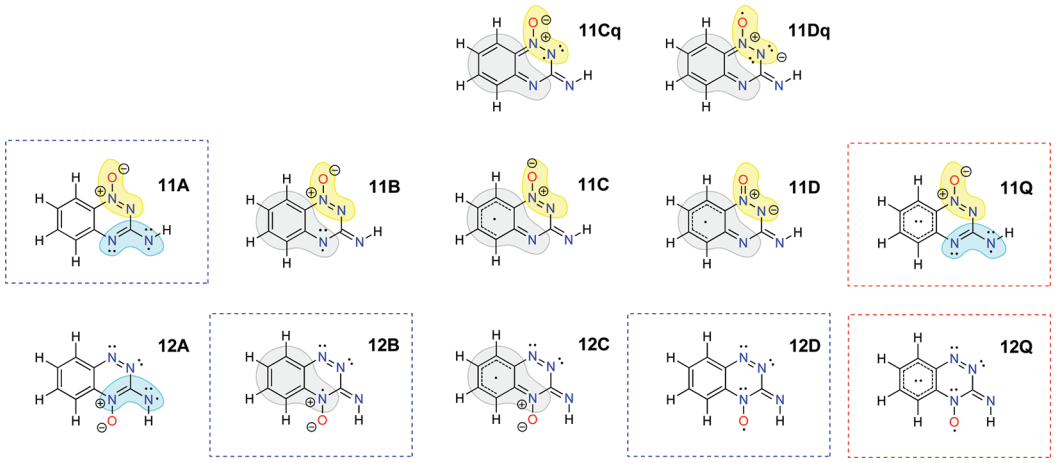

quinoid resonance structures, and the geometry of **11a** suggests that quinoid structures **11Cq** and **11Dq** are not important; the bond length $d(C_{Ar}–N1)$ greatly exceeds $d(C_{Ar}–N4)$ on the DFT and MP2 potential energy surfaces (DFT, $d(C_{Ar}–N1)$ = 1.426 Å, $d(C_{Ar}–N4)$ = 1.350 Å; MP2, $d(C_{Ar}–N1)$ = 1.414 Å, $d(C_{Ar}–N4)$ = 1.349 Å). Radical **11a** may still show spin density on O and N2 because the ONN moiety (yellow shading) is a 1,3-dipole, and 1,3-diradical forms contribute to its description.

The spin populations show two-thirds of a full spin on the NH group of **11a**, and this radical truly is an aminyl system (**11A**). Most of the α-spin remains in the triazene aminyl moiety (Σ_1 = 0.81) with some delocalization into the benzene ring (Σ_2 = 0.19). Hwoever, the major center of spin density in **12a** is the NO group (**12B**, **12D**) with a combined spin population of $\rho^S(NO)$ = 0.81, a much smaller spin density $\rho^S(NH)$ = 0.22 on the NH group, and hardly any spin delocalization into the benzene ring (Σ_2 = 0.07). The geometries reflect these electronic structures in that the exocyclic CN bond is much longer in **11a** than in **12a** (DFT, d(C3–NH) = 1.333 Å in **11a**, d(C3–NH) = 1.282 Å in **12a**; MP2, d(C3–NH) = 1.331 Å in **11a**, d(C3–NH) = 1.236 Å in **12a**).

The electronic structures of **11a** and **12a** are particularly interesting because neither one of them is a "normal" radical. Doublet radicals will frequently feature $1 < \Sigma_\alpha < 1.2$ and $-0.2 < \Sigma_\beta < 0$, and data of this type describe a "normal" system with one unpaired electron and some spin polarization. The phenyl radical **17** exemplifies such a case (Table 4). Instead, **11a** features a quartet instability ($\Sigma_\alpha \approx 2$, $\Sigma_\beta \approx -1$) in the QCI//DFT and QCI//MP2 densities. In the case of **12a**, the QCI density is sensitive to the structure. The QCI//MP2 wave function of **12a** is merely on the verge of quartet instability ($\Sigma_\alpha \approx 1.5$, $\Sigma_\beta \approx -0.5$), whereas the QCI//DFT wave function of **12a** shows quartet instability ($\Sigma_\alpha \approx 2.5$, $\Sigma_\beta \approx -1.5$) on the verge of further uncoupling. In cases of heavy spin polarization and/or spin delocalization, one has reasons to prefer DFT-optimized structures over MP2-optimized structures, and hence, we consider the QCI//DFT wave function to be physically more realistic.

The quartet instability in **11a** is associated with extreme spin polarization of the benzene ring; the C4a, HC5 and HC7 moieties all feature β-spin populations of almost 0.2 alternating with α-spin populations of almost equal magnitude on the C5a, HC6, and HC8 moieties. This spin polarization pattern results in almost one full α-spin and one full β-spin in the benzene ring. We suggest notation **11Q** to describe this spintronic situation (Scheme 3), that is, the benzene π-system uncouples to a singlet diradical. The spin polarization of the benzene ring in **12a** is analogous, and notation **12Q** can be used while keeping in mind that the uncoupling of the benzene π-system to a singlet diradical is accompanied by more spin polarization.

Table 4. Mulliken Spin Populations Computed at the QCI Level

	QCI//DFT			QCI//MP2		
atom/group[a]	**11a**	**12a**	**17**	**11a**	**12a**	**17**
O(N1), HO(N1)	−0.182		−0.022	−0.153		−0.015
N1	−0.165	0.362	0.063	−0.153	−0.051	0.057
N2	0.309	−0.360	0.009	0.268	0.066	−0.027
C3	−0.290	−0.047	−0.020	−0.279	−0.115	0.024
$(C3)NH_n$	0.648	0.177	0.001	0.666	0.221	0.003
N4	0.476	0.300	0.013	0.465	0.275	−0.015
O(N4), HO(N4)		0.495			0.537	
Σ_1	0.795	0.926	0.045	0.814	0.934	0.027
C4a	−0.213	−0.378	0.040	−0.186	−0.128	0.004
C5a	0.280	0.292	−0.093	0.249	0.120	−0.035
HC5	−0.197	−0.301	0.006	−0.159	−0.078	0.032
HC6	0.272	0.384	0.010	0.231	0.115	0.007
HC7	−0.178	−0.320	−0.051	−0.140	−0.080	−0.045
HC8, C8	0.241	0.397	1.044	0.191	0.116	1.009
Σ_2	0.205	0.074	0.955	0.186	0.066	0.973
Σ_α	2.224	2.406	1.186	2.071	1.451	1.137
Σ_β	−1.224	−1.406	−0.186	−1.071	−0.451	−0.137

[a] See Scheme 1 for atom numbering.

The spin density distributions of **11a** and **12a** (Figure 3) show large and alternating spin densities on all carbon atoms of their benzene rings with α-spin in the vicinities of **C5a**, **C6**, and **C8** and with β-spin in the basins of **C4a**, **C5**, and **C7**. Both isomers **11a** and **12a** also feature α-spin on the imine-NH group, on C3 and on N4, but only **11a** allows for spin alternation along every bond of the triazine ring.

Reaction Energies and Activation Barriers for Dehydration to Aminyl Radicals. We have shown above that doublets **11** and **12** are prone to quartet instabilities. This feature causes the theoretical level dependency of their relative stability and also affects the computed reaction energies of the dehydration reactions **3a** → **11a** + H_2O and **4b** → **12a** + H_2O.

dx.doi.org/10.1021/tx200546u | *Chem. Res. Toxicol.* 2012, 25, 634–645

Table 5. Mulliken Atom and Fragment Charges Computed at the QCI Level

	QCI//DFT			QCI//MP2		
atom/group[a]	11a	12a	17	11a	12a	17
O(N1), HO(N1)	−0.420		−0.463	−0.436		−0.427
N1	0.093	−0.229	0.136	0.094	−0.206	0.065
N2	−0.270	−0.216	−0.307	−0.268	−0.203	−0.285
C3	0.515	0.595	0.659	0.518	0.591	0.636
(C3)NH_n	−0.157	−0.189	−0.055	−0.157	−0.176	−0.052
N4	−0.440	−0.233	−0.539	−0.436	−0.270	−0.528
O(N4), HO(N4)		−0.380			−0.366	
Θ_1	−0.679	−0.651	−0.569	−0.684	−0.630	−0.590
C4a	0.214	0.344	0.240	0.208	0.364	0.228
C5a	0.269	0.128	0.209	0.276	0.110	0.240
HC5	0.075	0.067	0.087	0.083	0.048	0.090
HC6	0.032	0.017	0.002	0.028	0.023	−0.001
HC7	0.037	0.045	0.015	0.037	0.027	0.006
HC8, C8	0.053	0.050	0.015	0.053	0.057	0.028
$\Theta_2 = -\Theta_1$	0.679	0.651	0.569	0.684	0.630	0.590
Θ_+	1.287	1.246	1.365	1.296	1.221	1.292
$\Theta_- = -\Theta_+$	−1.287	−1.246	−1.365	−1.296	−1.221	−1.292

[a]See Scheme 1 for atom numbering.

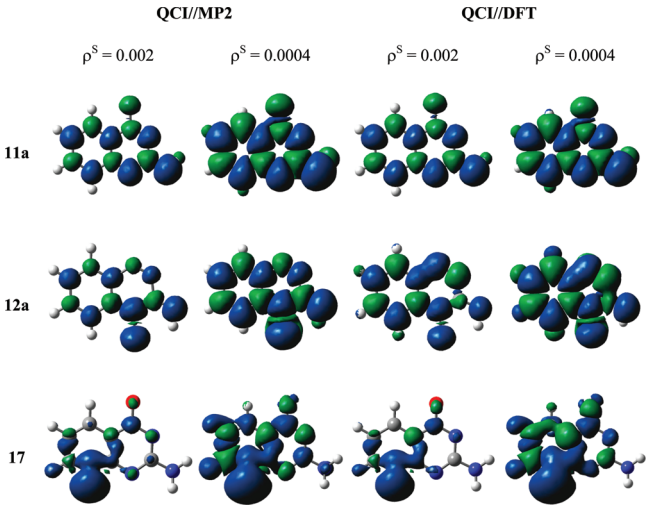

Figure 3. Spin-density distributions computed at the UQCISD level based on the MP2 (left) and DFT structures, respectively, for radicals **11**, **12**, and **17**. See text for details.

At the very least, the QCI level computations consistently show that the dehydration reactions clearly are exothermic and exergonic (Tables 1 and 2) and that dehydration therefore cannot be dismissed as a potential reaction channel. The QCI level dehydration free enthalpies corroborate and strengthen the conclusion reached by Anderson based on DFT levels data.[18]

The most pertinent values in the present context are the activation energies for the H-abstraction reactions **7** −(**TS3**) → **9** (Figure 1, solid curves) and **8** −(**TS4**) → **10** (Figure 1, dashed curves) and the $\Delta G'_{act}$(QCI//DFT) values are 21.5 and 22.4 kcal/mol, respectively, while the respective $\Delta G'_{act}$(QCI//MP2) values are 25.5 and 27.3 kcal/mol.

For isomers **3** and **4**, the PES analysis at the QCI//DFT level shows that (a) the activation barriers for H-abstraction from the NH_2 group are more than twice as high as the barriers for N−OH homolysis and that (b) the energy of the H-abstraction transition state structure is about the same as that of the homolysis transition state structure. This thermodynamic scenario allows for stepwise dehydration to occur in principle. Whether the stepwise dehydration does occur depends on the rate of separation of the products of N−OH homolysis. Dehydration could be quantitative if the H-abstraction can occur right after N−OH homolysis. The longer the hydroxyl aggregate exists, the more it will equilibrate thermally, and the ratio of the probabilities for dehydration relative to separation decreases as the hydroxyl aggregate becomes thermally equilibrated. It is important to realize that the separation of hydroxyl does not require the transport of OH by diffusion but that the high mobility of hydroxyl radical in water is due to low-barrier H-transfer between hydroxyl and water.[37] Recent isotopic labeling studies in the context of 3-methyl-1,2,4-benzotriazine 1,4-dioxide have provided evidence that HO· goes "free" without H-abstraction from the 3-methyl-1,2,4-benzotriazine 1-oxide metabolite.[38]

Reaction Energies and Activation Barriers for Dehydration to Phenyl Radicals. Dehydration with phenyl formation is included in the free enthalpy surface diagram (Figure 1; QCI//DFT in green and QCI//MP2 in orange), the overall reaction **3a** → 17 + H_2O is exothermic at every level (Tables 1 and 2), and this is in agreement with the computations by Anderson.[18] Our best value for dehydration with phenyl formation is $\Delta G'_{rxn}$(QCI//DFT) = −4.9 kcal/mol. Interestingly, the energy of the transition state structure **TS5** is rather similar to the energy of **TS3**, and we find $\Delta G'_{act}$(QCI//DFT) = 21.4 kcal/mol for the dehydration reaction and $\Delta G'_{act}$(QCI//DFT) = 14.4 kcal/mol for the reverse reaction 17 + H_2O → **13**.

The characteristics of the intrinsic reaction path computed for the formation of **17** can be consistent with the proposed formation of the spin-trap adduct of the kinetic dehydration product **17** if the spin-trap adduct is formed fast and irreversibly. However, if **17** had any significant lifetime, its fast back reaction to **13** would have to lead to the production of the thermodynamically preferred products **5** and/or **12**. This is a major cause for doubt about the relevance of **17** in the presence or absence of a spin trap because it is hard to imagine how any substrate could compete effectively with the back-reaction of **17** with water. The back-reaction 17 + H_2O → **13** is a pseudo-first order reaction with a small activation barrier (Figure 1). The capture of **17** by a spin trap also would have a low activation barrier, but it is a bimolecular reaction.

Alternatives to Dehydration: Spin Traps and Triazene Ring-Opening. To interpret the EPR spectra obtained by spin trapping of the reduction products of **1**, Anderson invoked radicals formed by addition of PBN to C3 of **3** and to C8 of the aryl radical **17**.[17,18] We have argued above that it is clear that a spin trap would not compete successfully for **17**, and we have shown in the preceding article[20] that **3** and **4** are not C3-centered radicals and, instead, that high spin densities occur in the (N1,O)-region of **3** and in the (N4,O)-region of **4**, respectively. The spin density analysis supports and corroborates the LDRMP-radical notation originally suggested by Lloyd et al.[6] for **3**, this conclusion is fully consistent with EPR spectra of the reduction product of **1**, and this finding casts doubt on the assumption that the spin-trap PBN would add to C3 of **3**.

The pK_a(**3**) = 6 was reported based on the observation of the disproportionation reaction of **3** to **5** and **1**. Our studies show very low proton affinities of radical anion **2** and suggest that the

dx.doi.org/10.1021/tx200546u | Chem. Res. Toxicol. 2012, 25, 634−645

Scheme 4. CN Bond Dissociations of 2 Leading to Phenyl (A,B) and C3-Centered (D) Radicals[a]

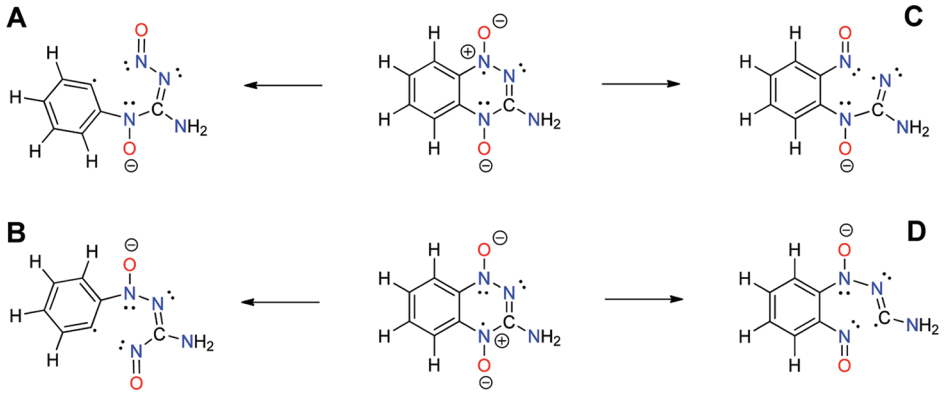

[a]The NN bond dissociation leads to an N2-centered radical (**C**). Paths similar to **A** (**B**) and **C** (**D**) may occur in the respective protonated species **3** (**4**).

pK_a of radical [**2**+H] might even be lower than 6. In neutral or basic solution, one should expect [**2**]/[**3**] ≫ 1, and EPR measurements might report on spin-trap adducts of radical anion **2**, rather than the neutral radical **3**.

Faced with these inconsistencies, one must ask whether there might be reaction channels for the generation of aryl radical species other than the proposed dehydration pathway. One possible resolution consists in the dissociation of the C5a−N1 bond (**A**) or of the C4a−N4 bond (**B**) in **2** (Scheme 4). Dissociations **A** and **B** turn an (N,O)-centered radical into a nitroso compound and a phenyl radical. The (N4,O) region does not participate in **A**, and essentially the same process might occur for **3a**. Similarly, the (N1,O) region does not participate in **B**, and this dissociation might occur in **4b**. We scanned the potential energy surfaces of **2** and of the protonated systems **3** or **4** as a function of the C5a−N1 and/or C4a−N4 bonds at the B3LYP/6-31G* level, and the results are shown in Figure 4.

Stretching the C5a−N1 bond has much the same effect in **2** and **3**, and an elongation of about 1 Å requires roughly 50 kcal/mol. Similarly, an elongation of the C4a−N4 bond in **2** or **4** by about 1 Å requires >60 kcal/mol. None of these modes of dissociation will occur *as a unimolecular reaction*. However, the important point here is the recognition that elongation of the C5a−N1 bond converts the (N1,O)-centered radicals of **2** and **3** into latent C5a-centered phenyl radicals (**A**) and that C4a−N4 bond elongation converts the (N4,O)-centered radicals of **2** and **4** into latent (or nascent) C4a-centered phenyl radicals (**B**). The activation barriers of the *bimolecular reactions* of a spin-trap molecule with **2** or **3** at C5a or with **2** or **4** at C4a, respectively, would be much less than the energy required for unassisted bond dissociation.

In the same spirit, we considered the dissociations of the N2−N1 bond (**C**) and of the C3−N4 bond (**D**) in **2** (Scheme 4) to convert an (N,O)-centered radical into either an N2- or a C3-centered radical, respectively. As with **A** and **B**, the dissociation **C** also may occur in **3a**, while process **D** also might occur in **4b**. The scans of the B3LYP/6-31G* potential energy surfaces of **2** and of **3** or **4** as a function of the N2−N1 and/or C3−N4 bonds are shown in Figure 4b. Stretching the N2−N1 bond is quite different in **2** and **3**: An elongation of about 1 Å requires only about 35 kcal/mol in **2**, while the same elongation requires close to 60 kcal/mol in **3**. An elongation of the C3−N4 bond by 1 Å requires about 60 kcal/mol in **2** or **4**. While the *unimolecular* dissociations will not occur at the temperatures of spin-trapping experiments, the important point is again that the *bimolecular reactions* of a spin trap with **2** or **3** at N2 or with **2** or **4** at C3, respectively, would require much less activation energy than unassisted bond dissociation. The plots in Figure 4 show that bond elongation by about 0.5 Å requires about 35 kcal/mol and that the barrier of the bimolecular reaction would be lowered by the partial formation of the new bond. While the *addition* of spin traps to C3 of **2** or protonated **2** is not likely, these results suggest that spin traps may react at C3 by *substitution*, i.e., addition to C3 with concomitant triazene ring-opening.

With a view to bimolecular reactions, the segments with bond elongations of up to 0.6 Å are the most significant regions of the dissociation paths **A**−**D**. In addition to the B3LYP/6-31G* level, we also computed the important segment of each of the four paths of the radical anion **2** with the addition of diffuse functions to the basis set at the DFT level (B3LYP/6-31+G*) and at the QCI level (QCISD/6-31+G*//B3LYP/6-31+G*). The results are shown in Figure 5; the theoretical level effects are found to be modest, and the higher level QCI data corroborate the DFT data.

CONCLUSIONS

The theoretical study of TPZ chemistry is nontrivial because extended conjugation and near-degeneracies cause complicated patterns of spin delocalization and spin polarization including quartet instabilities of doublet radicals. We presented results of density functional theory, of second-order and higher-order perturbation theory, and of quadratic configuration interaction theory. Relative and reaction energies, activation energies, populations, and spin density distributions computed at the QCI//DFT and QCI//MP2 levels were presented. Variational CI theory is essential for the adequate computation of spin-density distributions, the QCI results are qualitatively similar, and we tend to favor QCI//DFT over QCI//MP2 results.

The doublet radical **17** is a normal spin-polarized radical (Σ_α < 1.2 and Σ_β > −0.2). The doublet radicals **11** and **12** feature quartet instabilities; **11** is a doublet triradical ($\Sigma_\alpha \approx 2$, $\Sigma_\beta \approx -1$), and **12** is is a heavily spin-polarized doublet triradical ($\Sigma_\alpha \approx 2.5$, $\Sigma_\beta \approx -1.5$). Most of the net electron spin of **11** and **12** is located in the triazine moiety, and this spin density causes the uncoupling of electrons in the benzene ring.

dx.doi.org/10.1021/tx200546u | *Chem. Res. Toxicol.* 2012, 25, 634−645

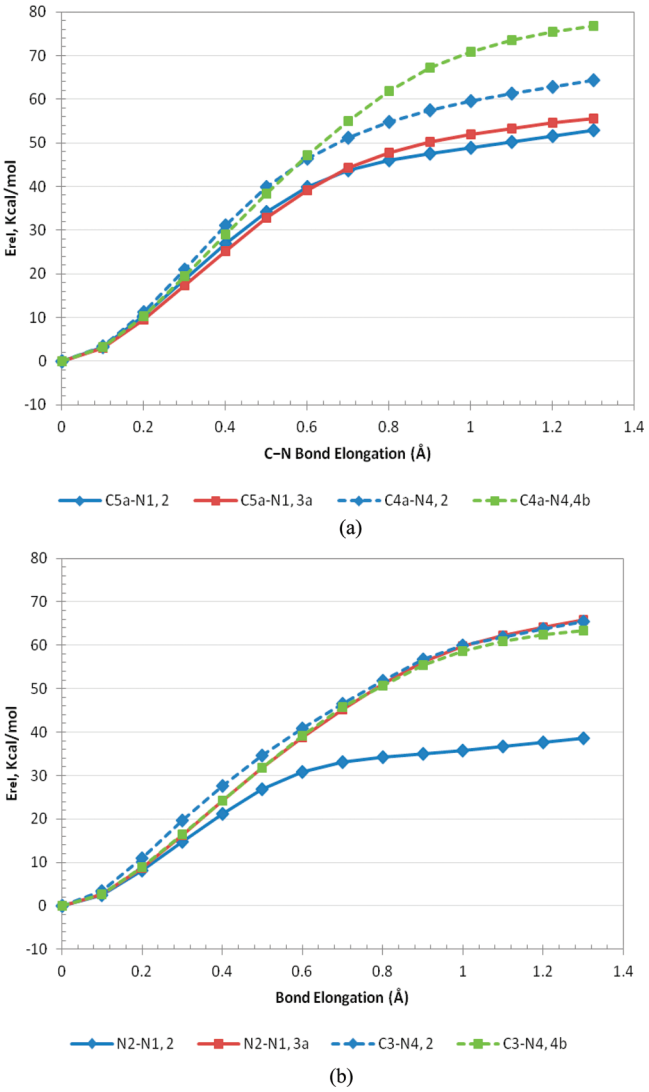

Figure 4. Scans of the potential energy surfaces of **2** and of **3** or **4** as a function of X–N(O) bond elongation. Energies are in kcal/mol relative to the radical anion **2** or the protonated anion **3** or **4**, respectively. (a) Path **A**: C5a–N1 bond elongation in **2** (blue, diamond, solid) and **3** (red, square, solid). Path **B**: C4a–N4 bond elongation in **2** (blue, diamond, dashed) and **4** (green, square, dash). (b) Path **C**: N2–N1 bond elongation in **2** (blue, diamond, solid) and **3** (red, square, solid). Path **D**: C3–N4 bond elongation in **2** (blue, diamond, dashed) and **4** (green, square, dash).

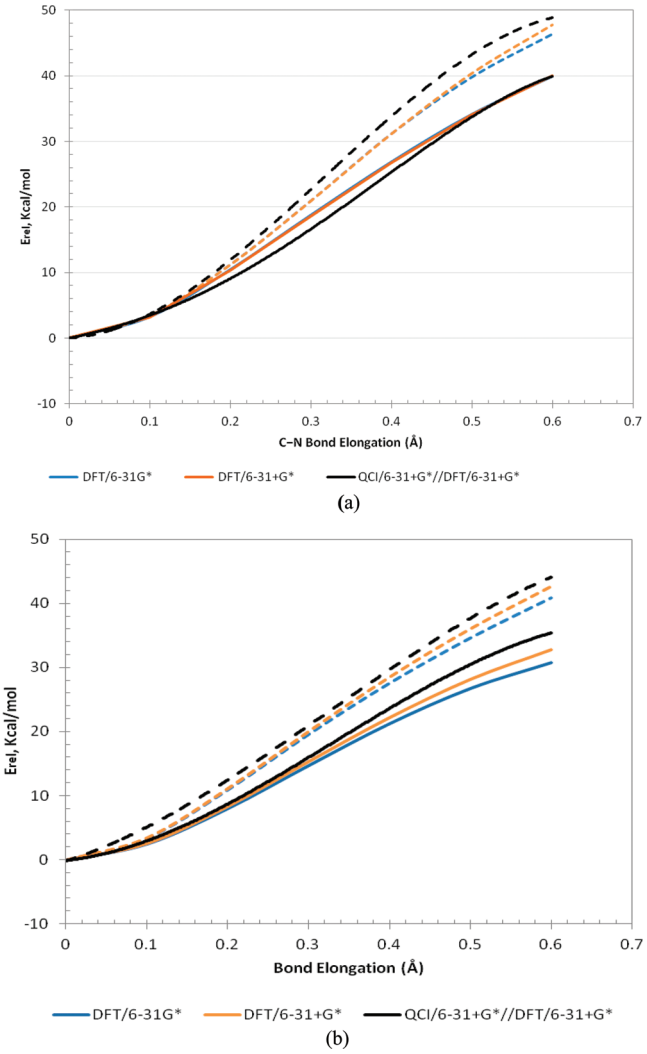

Figure 5. Scans of the potential energy surfaces of **2** as a function of X–N(O) bond elongation in kcal/mol relative to the radical anion **2** for three theoretical levels DFT/6-31G* (blue), DFT/6-31+G* (orange), and QCISD/6-31+G*//DFT/6-31+G* (black). (a) Path **A**: C5a–N1 bond elongation (solid). Path **B**: C4a–N4 bond elongation (dashed). (b) Path **C**: N2–N1 bond elongation in **2** (solid). Path **D**: C3–N4 bond elongation in **2** (dashed).

We have explored the stepwise paths for the dehydrations to aminyl radicals (**3a** −(**TS1**) → **7** −(**TS3**) → **9** → **11a** + H_2O and **4b** −(**TS2**) → **8** −(**TS4**) → **10** → **12a** + H_2O), and one path to a phenyl radical **17** (**3a** −(**TS1**) → **13** −(**TS5**) → **15** → **17** + H_2O). All stationary structures of OH aggregates of **5** and **6**, of H_2O aggregates of **11**, **12**, and **17**, and of the transition state structures for H-abstraction were located and characterized by vibrational analysis. The computed reactions energies and the activation barriers allow for the dehydration reactions to occur in principle. The productivity of all of these dehydration paths should be seriously impeded, however, because the hydroxyl radical may escape its weakly bound aggregates with **5** or **6** prior to H-abstraction. Indeed, isotopic labeling studies in the context of 3-methyl-1,2,4-benzotriazine 1,4-dioxide have provided evidence that HO· escapes without H-abstraction from the 3-methyl-1,2,4-benzotriazine 1-oxide metabolite.[37] Moreover, the dehydration leading to aryl formation is endothermic relative to aggregate **7**, and the most likely reaction of the hydrate of **17** is its back-reaction to **7**. The results of the potential energy surface analyses have several important implications.

If **3** and/or **4** are formed by protonation of **2**, N–OH homolysis is the most likely option. Some dehydration might occur by a stepwise process after N–OH homolysis, but such dehydration can never be quantitative, and the dehydration to phenyl radical should be entirely unproductive.

With a view to plausible scenarios that allow for aryl radical species without having to invoke dehydration, we considered the bond dissociations **A**–**D** in **2** and the analogous reactions of **3** and **4**. Scans of the potential energy surfaces of **2**–**4** as a function of the (O)N1–Y (Y = C5a, N2) and (O)N4–Z (Z = C4a, C3) bond lengths show that the elongation of any one of these bonds by 0.5 Å requires less than 25 kcal/mol. This finding strongly suggests the possibility of bimolecular reactions

dx.doi.org/10.1021/tx200546u | *Chem. Res. Toxicol.* 2012, 25, 634–645

of the spin trap molecules with **2**−**4** concomitant with triazene ring-opening.

Comprehensive experimental studies are needed of the structures and hyperfine coupling constants of the spin trap adducts together with theoretical studies of their potential energy surfaces and their spin density distributions. It is hoped that the results of the present study provides a suitable conceptual framework for these mechanistic studies.

■ ASSOCIATED CONTENT

Supporting Information

Two tables with energies and thermochemical parameters computed at the levels B3LYP/6-31G* and QCI/6-31G*//B3LYP/6-31G* and MP2(full)/6-31G* and QCI/6-31G*//MP2(full)/6-31G*, one figure showing DFT and MP2 spin density distributions of **11a**, **12**, and **17**, and Cartesian coordinates of all optimized structures. This material is available free of charge via the Internet at http://pubs.acs.org.

■ AUTHOR INFORMATION

Corresponding Author

* E-mail: glaserr@missouri.edu (R.G.); gatesk@missouri.edu (K.S.G.).

Author Contributions

R.G. and K.S.G. designed the study, J.Y. and R.G. conducted the research, and R.G. wrote the article with assistance from J.Y. All authors edited and approved the final manuscript.

Notes

The authors declare no competing financial interest.

■ ABBREVIATIONS

EPR, electron paramagnetic resonance; RHF, restricted Hartree−Fock; ROHF, restricted open-shell Hartree−Fock; UHF, unrestricted Hartree−Fock; PUHF, projected UHF; MPx, Møller−Plesset perturbation theory of x-th order; UMPx, unrestricted MPx theory; PUMPx, projected UMPx; DFT, density functional theory; QCISD, quadratic configuration theory with single and double excitations; RQCISD, restricted QCISD; UQCISD, unrestricted QCISD; DMSO, dimethyl sulfoxide; TPZ, tirapazamine; BTZ, benzotriazinyl; BTO, 1,2,4-benzotriazine 1,4-*N*,*N*-dioxide

■ REFERENCES

(1) (a) Brown, J. M., and Wilson, W. R. (2004) Exploiting tumour hypoxia in cancer treatment. *Nat. Rev. Cancer 4*, 437−447. (b) Brown, J. M. (1999) The hypoxic cell: a target for selective cancer therapy—Eighteenth Bruce F. Cain Memorial Award lecture. *Cancer Res. 59*, 5863−5870. (c) Denny, W. A., and Wilson, W. R. (2000) Tirapazamine: a bioreductive anticancer drug that exploits tumour hypoxia. *Expert Opin. Invest. Drugs 9*, 2889−2901. (d) Vaupel, P., Kallinowski, F., and Okunieff, P. (1989) Blood flow, oxygen and nutrient supply, and metabolic microenvironment of human tumors: a review. *Cancer Res. 49*, 6449−6465. (e) Wilson, W. R. (1992) Tumor Hypoxia: Challenges for Cancer Chemotherapy, in *The Search for New Anticancer Drugs*, (Waring, M. J., and Ponder, B. A. J.., Eds.) Kluwer Academic: Lancaster, PA. (f) Zeman, E. M., Brown, J. M., Lemmon, M. J., Hirst, V. K., and Lee, W. W. (1986) SR-4233: a new bioreductive agent with high selective toxicity for hypoxic mammalian cells. *Int. J. Radiat. Oncol. Biol. Phys. 12*, 1239−1242.

(2) Laderoute, K. (1988) Molecular mechanisms for the hypoxia-dependent activation of 3-amino-1,2,4-benzotriazine-1,4-dioxide (SR 4233). *Biochem. Pharmacol. 37*, 1487−1495.

(3) Laderoute, K. L., Wardman, P., and Rauth, M. (1988) Molecular mechanisms for the hypoxia-dependent activation of 3-amino-1,2,4-benzotriazine-1, 4-dioxide (SR 4233). *Biochem. Pharmacol. 37*, 1487−1495.

(4) Wardman, P., Priyadarsini, K. I., Dennis, M. F., Everett, S. A., Naylor, M. A., Patel, K. B., Stratford, I. J., Stratford, M. R. L., and Tracy, M. (1996) Chemical properties which control selectivity and efficacy of aromatic N-oxide bioreductive drugs. *Br. J. Cancer 74*, S70−S74.

(5) Priyadarsini, K. I., Tracy, M., and Wardman, P. (1996) The one-electron reduction potential of 3-amino-1,2,4-benzotriazine 1,4-dioxide (tirapazamine): a hypoxia-selective bioreductive drug. *Free Radical Res. 25*, 393−399.

(6) Lloyd, R. V., Duling, D. R., Rumyanseva, G. V., Mason., R. P., and Bridson, P. K. (1991) Microsomal Reduction of 3-Amino-1,2,4-Benzotriazine 1,4-Dioxide to a free Radical. *Mol. Pharmacol. 40*, 440−445.

(7) Patterson, L. H., and Taiwo, F. A. (2000) Electron Paramagnetic Resonance Spectrometry Evidence for Bioreduction of Tirapazamine to Oxidising Free Radicals Under Anaerobic Conditions. *Biochem. Pharmacol. 60*, 1933−1935.

(8) Daniels, J. S., and Gates, K. S. (1996) DNA cleavage by the antitumor agent 3-amino-1,2,4-benzotrizaine 1,4-dioxide (SR4233): evidence for involvement of hydroxyl radical. *J. Chem. Soc. 118*, 3380−3385.

(9) Hwang, J. -T., Greenberg, M., Fuchs, T., and Gates, K. S. (1999) Reaction of the hypoxia-selective antitumor agent tirapazamine with a C1′-radical in single-stranded and double-stranded DNA: the drug and its metabolites can serve as surrogates for molecular oxygen in radical-mediated DNA damage reactions. *Biochemistry 38*, 14248−14255.

(10) Fuchs, T., Chowdhury, G., Barnes, C. L., and Gates, K. S. (2001) 3-amino-1,2,4-benzotriazine 4-oxide: characterization of a new metabolite arising from bioreductive processing of the antitumor agent 3-amino-1,2,4-benzotrizine 1,4-dioxide (Tirapazamine). *J. Org. Chem. 66*, 107−114.

(11) Kotandeniya, D., Ganley, B., and Gates, K. S. (2002) Oxidative DNA base damage by the antitumor agent 3-amino-1,2,4-benzotriazine 1,4-dioxide (Tirapazamine). *Bioorg. Med. Chem. Lett. 12*, 2325−2329.

(12) Birincioglu, M., Jaruga, P., Chowdhury, G., Rodriguez, H., Dizdaroglu, M., and Gates, K. S. (2003) DNA base damage by the antitumor agent 3-amino-1,2,4-benzotrizine 1,4-dioxide (Tirapazamine). *J. Chem. Soc. 125*, 11607−11615.

(13) Zagorevski, D., Yuan, Y., Fuchs, T., Gates, K. S., Song, M., Breneman, C., and Greenlief, C. M. (2003) A mass spectrometry study of tirapazamine and its metabolites: insights into the mechanism of metabolic transformations and the characterization of reaction intermediates. *J. Am. Soc. Mass Spectrom. 14*, 881−892.

(14) Chowdhury, G., Junnutula, V., Daniels, J. S., Greenberg, M. M., and Gates, K. S. (2007) DNA strand damage product analysis provides evidence that the tumor cell-specific cytotoxin tirapazamine produces hydroxyl radical and acts as a surrogate for O_2. *J. Chem. Soc. 129*, 12870−12877.

(15) Chowdhury, G., Sarkar, U., Pullen, S., Wilson, W. R., Rajapakse, A., Fuchs-Knotts, T., and Gates, K. S. (2012) Strand Cleavage by the phenazine di-N-oxide natural product myxin under both aerobic and anaerobic conditions. *Chem. Res. Toxicol. 25*, 197−206.

(16) Anderson, R. F., Shinde, S. S., Hay, M. P., Gamage, S. A., and Denny, W. A. (2003) Activation of 3-amino-1,2,4-benzotriazine 1,4-dioxide antitumor agents to oxidizing species following their one-electron reduction. *J. Chem. Soc. 125*, 748−756.

(17) Shinde, S. S., Hay, M. P., Patterson, A. V., Denny, W. A., and Anderson, R. F. (2009) Spin trapping of radicals other than the $^{\bullet}OH$ radical upon reduction of the anticancer agent tirapazamine by cytochrome P_{450} reductase. *J. Am. Chem. Soc. 131*, 14220−14221.

(18) Shinde, S. S., Maroz, A., Hay, M. P., Patterson, A. V., Denny, W. A., and Anderson, R. F. (2010) Characterization of radicals formed following enzymatic reduction of 3-substituted analogues of the hypoxia-selective cytotoxin 3-amino-1,2,4-benzotriazine 1,4-dioxide (tirapazamine). *J. Am. Chem. Soc. 132*, 2591−2599.

(19) (a) Li, L.-C., Zha, D., Zhu, Y.-Q., Xu, M.-H., and Wong, N.-B. (2005) Theoretical study of the mechanism of hydroxyl radical release

from tirapazamine's undergoing enzymatic catalysis. *Chem. Phys. Lett. 408*, 329−334. (b) Li *et al.* also studied the reactions of **5** and **6** to 3-amino-1,2,4-benzotriazine by another reduction/protonation/homolysis sequence.

(20) Yin, J., Glaser, R., and Gates, K. S. (2012) Electron and spin-density analysis of tirapazamine reduction chemistry. *Chem. Res. Toxicol.*, DOI: 10.1021/tx2005458.

(21) (a) Pogozelski, W. K., McNeese, T. J., and Tullius, T. D. (1995) What species is responsible for strand scission in the reaction of $[Fe(EDTA)]^{2-}$ and H_2O_2 with DNA? *J. Am. Chem. Soc. 117*, 6428−6433. (b) Pratviel, G., Bernadou, J., and Meunier, B. (1995) Carbon—hydrogen bonds of DNA sugar units as targets for chemical nucleases and drugs. *Angew. Chem., Int. Ed. Engl. 34*, 746−769. (c) Evans, M. D., Dizdaroglu, M., and Cooke, M. S. (2004) Oxidative DNA damage and disease: induction, repair and significance. *Mutat. Res. 567*, 1−61.

(22) Laderoute, K. R., and Rauth, A. M. (1986) Identification of two major reduction products of the hypoxic cell toxin 3-amino-1,2,4-benzotriazine-1,4-dioxide. *Biochem. Pharmacol. 35*, 3417−3420.

(23) Singh, R. J., Karoui, H., Gunther, M. R., Beckman, J. S., Mason, P. P., and Kalyanaraman, B. (1998) Reexamination of the mechanism of hydroxyl radical adducts formed from the reaction between familial amyotrophic lateral sclerosis-associated Cu,Zn superoxide dismutase mutants and H_2O_2. *Proc. Natl. Acad. Sci. U.S.A. 95*, 6675−6680.

(24) A nonpolar dehydration reaction could involve a concerted elimination if both bond homolyses required high activation energies. Since the N−OH homolysis requires relatively little activation energy, a concerted mechanism does not provide an energetic benefit but would only add an entropic burden.

(25) Frisch, M. J., Trucks, G. W., Schlegel, H. B., Scuseria, G. E., Robb, M. A., Cheeseman, J. R., Scalmani, G., Barone, V., Mennucci, B., Petersson, G. A., Nakatsuji, H., Caricato, M., Li, X., Hratchian, H. P., Izmaylov, A. F., Bloino, J., Zheng, G., Sonnenberg, J. L., Hada, M., Ehara, M., Toyota, K., Fukuda, R., Hasegawa, J., Ishida, M., Nakajima, T., Honda, Y., Kitao, O., Nakai, H., Vreven, T., Montgomery, J. A., Jr., Peralta, J. E., Ogliaro, F., Bearpark, M., Heyd, J. J., Brothers, E., Kudin, K. N., Staroverov, V. N., Kobayashi, R., Normand, J., Raghavachari, K., Rendell, A., Burant, J. C., Iyengar, S. S., Tomasi, J., Cossi, M., Rega, N., Millam, J. M., Klene, M., Knox, J. E., Cross, J. B., Bakken, V., Adamo, C., Jaramillo, J., Gomperts, R., Stratmann, R. E., Yazyev, O., Austin, A. J., Cammi, R., Pomelli, C., Ochterski, J. W., Martin, R. L., Morokuma, K., Zakrzewski, V. G., Voth, G. A., Salvador, P., Dannenberg, J. J., Dapprich, S., Daniels, A. D., Farkas, O., Foresman, J. B., Ortiz, J. V., Cioslowski, J., and Fox, D. J. (2009) *Gaussian 09*, revision B.01, Gaussian, Inc., Wallingford, CT.

(26) Becke, A. D. (1993) Density-functional thermochemistry. III. The role of exact exchange. *J. Chem. Phys. 98*, 5648−5652.

(27) (a) Pople, J. A. (1999) Nobel lecture: Quantum chemical models. *Rev. Mod. Phys. 71*, 1267−1274. (b) Binkley, J. S., and Pople, J. A. (1975) Møller-Plesset theory for atomic ground-state energies. *Int. J. Quantum Chem. 9*, 229−236.

(28) He., Z., Kraka, E., and Cremer, D. (1996) Application of quadratic CI with singles, doubles, and triples (QCISDT): an attractive alternative to CCSDT. *Int. J. Quantum Chem. 57*, 157−172.

(29) Glaser, R., and Choy, G. S.-C. (1993) Electron and spin density analysis of spin-projected unrestricted Hartree-Fock density matrixes of radicals. *J. Phys. Chem. 97*, 3188−3198.

(30) Sui, Y., Glaser, R., Sarkar, U., and Gates, K. (2007) Stabilities and spin distributions of benzannulated benzyl radicals. *J. Chem. Theory Comput. 3*, 1091−1099.

(31) Glaser, R., Sui, Y., Sarkar, U., and Gates, K. (2008) Electronic structures and spin topologies of γ-picoliniumyl radicals. A study of the homolysis of *N*-methyl-γ-picolinium and of benzo-, dibenzo-, and naphthoannulated analogs. *J. Phys. Chem. A 112*, 4800−4814.

(32) Schlegel, H. B., and McDouall, J. J. (1991) Do You Have SCF Stability and Convergence Problems? in *Computational Advances in Organic Chemistry* (Ögretir, C., and Csizmadia, I. G., Eds.) pp 167−185, Kluwer Academic, The Netherlands.

(33) (a) Chan, Wai-To, and Hamilton, I. P. (2003) Mechanisms for the ozonolysis of ethene and propene: reliability of quantum chemical predictions. *J. Chem. Phys. 118*, 1688−1701. (b) Pulay, P., and Liu, R. F. (1990) Methods for finding unrestricted Hartree-Fock solutions and multiple solutions. *J. Phys. Chem. 94*, 5548−5551. (c) Raghavachari, K., Trucks, G. W., Pople, J. A., and Replogle, E. (1989) Highly correlated systems: structure, binding energy and harmonic vibrational frequencies of ozone. *Chem. Phys. Lett. 158*, 207−212.

(34) (a) Kuz'mitskii., V. A. (2004) Instability of the molecular structure of monobenzoporphin to the alternation of the macrocycle bond lengths and its manifestation in the electronic spectra. *J. Appl. Spectrosc. 71*, 777−787. (b) Colvin, M. E., Janssen, C. L., Seidl, E. T., Nielsen, I. M. B., and Melius, C. F. (1998) Energies, resonance and UHF instabilities in polycyclic aromatic hydrocarbons and linear polyenes. *Chem. Phys. Lett. 287*, 537−541.

(35) (a) Sheka, E. F., and Chernozatonskii, L. A. (2010) Broken symmetry approach and chemical susceptibility of carbon nanotubes. *Intl. J. Quant. Chem. 110*, 1466−1480. (b) Sheka, E. F. (2007) Chemical susceptibility of fullerenes in view of Hartree-Fock approach. *Intl. J. Quant. Chem. 107*, 2803−2816.

(36) Glaser, R., and Prugger, K. (2012) Iodine bonding stabilizes iodomethane in MIDAS pesticide. Theoretical study of intermolecular interactions between iodomethane and chloropicrin. *J. Agric. Food Chem. 60*, 1776−1787.

(37) Codorniu-Hernández, E., and Kusalik, P. G. (2012) Mobility mechanism of hydroxyl radicals in aqueous solution via hydrogen transfer. *J. Am. Chem. Soc. 134*, 532−538.

(38) Junnotula, V., Sarkar, U., Sinha, S., and Gates, K. S. (2009) Initiation of DNA strand cleavage by 1,2,4-benzotriazine 1,4-dioxides: mechanistic insight from studies of 3-methyl-1,2,4-benzotriazine 1,4-dioxide. *J. Am. Chem. Soc. 131*, 1015−1024.